

UV Extinction as a More Fundamental Measure of Dust than $E(B - V)$ or A_V

ROBERT E. BUTLER ¹ AND SAMIR SALIM ¹

¹*Indiana University
727 E. Third Street
Bloomington, IN 47405*

ABSTRACT

The gas-to-dust ratio of reddened stars in the Milky Way (MW), the Magellanic Clouds, and in general is usually expressed as a linear relation between the hydrogen column density, $N(\text{H})$, and the reddening, $E(B - V)$, or extinction in the V band (A_V). If the extinction curve was truly universal, the strength of the relationship and the linearity would naturally be maintained for extinction at any wavelength, and also for $N(\text{H})$ vs. $E(B - V)$. However, extinction curves vary within the Milky Way, and there is no reason why, except by chance, either $E(B - V)$ or A_V would be the most physical measure of dust column density. In this paper, we utilize for the first time full extinction curves to 41 MW sightlines and find that the scatter between $N(\text{H})$ and extinction is minimized—and the relation becomes linear—for extinction at $2900 \pm 160 \text{ \AA}$. Scatter and nonlinearity increase at longer wavelengths and are especially large for near-IR extinction. We conclude that near-UV extinction is a superior measure of the dust column density for MW dust. We provide new, non-linear gas-to-dust relations for various dust tracers. We also find that the very large discrepancy between MW and SMC gas-to-dust ratios of 0.9 dex in $N(\text{H})/E(B - V)$ is reduced to 0.7 dex for far-UV extinction, which matches the difference in cosmic abundances of carbon between the two galaxies, and therefore confirms that $N(\text{C})$ is the preferred measure of the gas in the gas-to-dust ratio, even though it may not be a convenient one.

Keywords: TBD

1. INTRODUCTION

A practical quantification of the amount of dust lying between the observer and a star or galaxy is of great importance for a wide range of Galactic and extragalactic studies, including efforts to model galaxy evolution (Galliano et al. 2018; Salim & Narayanan 2020). Ideally, the dust should be measured as the dust column density (N_d), and consequently, the gas-to-dust ratio should be expressed as $N(\text{H})/N_d$ (or equivalently m_{H}/m_d), where $N(\text{H})$ represents hydrogen column density between the observer and the emitter. However, measuring dust column density is not straightforward. In situations where all of the dust lies in front of the reddened object, one can use far-infrared emission to obtain dust column density. IR maps are the basis for the MW reddening maps of Schlegel et al. (1998), which are widely used to correct

(“deredden”) the fluxes of extragalactic objects. However, when the dust is situated both in front of and behind a reddened star in the Galaxy, or when a stellar population is mixed with dust in an external galaxy (galaxy attenuation), IR emission overestimates the dust column. We must then use other ways to estimate it.

Traditionally, it is the reddening ($E(B - V)$), i.e., the difference in extinction between B and V bands ($A_B - A_V$) which is most commonly used as a measure of dust. Consequently, $N(\text{H})/E(B - V)$ is used as a measure of the gas-to-dust ratio (e.g., Savage et al. 1977; Bohlin et al. 1978). However, there is no reason why $E(B - V)$ would be a better measure of column density—and, by extension, better correlate with $N(\text{H})$ —than A_V (e.g., Zhu et al. 2017), or extinction at some other wavelength (A_λ). If the extinction curve was universal at all wavelengths, i.e., if A_λ normalized at some wavelength was the same for all stars ($A_\lambda/A_V = \text{const.}$), the question of the most fundamental measure of dust would be moot. A_λ would simply be proportional to $E(B - V)$, with the same coefficient of proportionality for all stars.

Equivalently, this is to say that the R_V parameter is constant, because by definition $A_V = R_V E(B - V)$. In reality, R_V —and therefore the shape of the extinction curve—can vary significantly from one sightline to another, especially for high-opacity regions in the Milky Way ($2 < A_V < 6$; e.g., Cardelli et al. 1989; Valencic et al. 2004). The diversity of extinction curves implies that if $N(\text{H})$ is best correlated with some $A_{\lambda, \text{best}}$, it will *not* be so for other A_λ .

Currently, it is unknown which extinction (A_λ) best correlates with $N(\text{H})$ and is therefore the best measure of the dust column. Consequently, we also do not know if the correlation at this best A_λ is better or worse than with $E(B - V)$. From a purely practical standpoint, $E(B - V)$ is the most convenient measure, because its determination (unlike that of arbitrary A_λ) does not require multiwavelength photometry extending into the near-IR (where extinction tends towards zero).

It has been asserted by Jura (1980) that there is no reason why either $E(B - V)$ or A_V would be the best measure of dust. Instead, Jura proposed that the fundamentally better motivated measure of dust may be extinction in the near-IR (NIR), such as $A_{3.6\mu\text{m}}$ (L -band), but this proposal has not been confirmed empirically.

To our knowledge, there has been only one study that attempted to predict the wavelength at which extinction is the best measure of dust. Kim & Martin (1996) used the Kramers-Kronig approach (Purcell 1969), together with dust grain distribution models for different values of R_V , to determine the wavelength at which the gas-to-dust ratio is independent from R_V —a necessary condition for the minimization of scatter between A_λ and $N(\text{H})$. For MW dust they find that this should happen at approximately 3600 Å (near U band). However, this result has not been widely accepted or even discussed in subsequent literature, and in any case the question has never been put to an empirical test. The aim of this paper is to do so.

The ancillary goal of this paper is to try to find a unifying framework for disparate gas-to-dust ratios in the MW and SMC. The gas-to-dust ratio, expressed using the column density of hydrogen, is to first order constant within the Milky Way (Bohlin et al. 1978). However, the gas-to-dust ratio is ~ 0.9 dex higher in the SMC, at least when $E(B - V)$ is used as the tracer of dust. This great discrepancy suggests that the fundamental relation (one that would not change from galaxy to galaxy) could involve the column density of some element that is more directly related to the dust, in place of hydrogen (e.g., Clayton & Martin 1985; Mathis 1990; Draine 2003; Welty et al. 2012). The best candidate for this alternative abundance is carbon, the cosmic abundance of

which is 0.6 dex lower in the SMC than in the MW. The difference in abundance goes a significant way toward explaining the difference in $N(\text{H})/E(B - V)$ gas-to-dust ratios, but is still 0.3 dex short. Here we investigate if the solution to this discrepancy lies in $E(B - V)$ not being the most appropriate measure of dust.

In this work we take advantage of the fact that detailed extinction curves are available in the literature for a relatively large number of MW stars. We use Fitzpatrick & Massa (2007, hereafter FM07) extinction curve parameters in combination with hydrogen column densities from Gudennavar et al. (2012, hereafter G12) to evaluate across wavelengths from the UV to the NIR which A_λ is the most fundamental measure of dust. Section 2 describes these sources of data. Section 3 describes how our sample was created, along with the methods used to determine the best measure of dust. The plausibility of metallicity driving the scatter in the $N(\text{H})$ vs. A_λ relation is also explored. In Section 4 we discuss our results in the context of prior results in the literature. The relation of our results to extinction and metallicity in the SMC is also discussed there.

2. DATA AND SAMPLE

We draw the main data for this study from two sources: FM07 provides extinction curve parameters, and G12 gives column densities for hydrogen and metals. FM07 represents one of the largest samples of full extinction curves for Milky Way sightlines obtained to date. G12 is the largest compilation of interstellar column density measurements from the literature, containing measurements toward over 3000 stars (most in the MW and some in the Magellanic Clouds) across ~ 50 different species.

2.1. Extinction

FM07 mostly contains B and late O stars for which the authors were able to gather UV through IR data: UV spectrophotometry from the *International Ultraviolet Explorer (IUE)*, UBV photometry from various sources, and JHK photometry from the Two-Micron All Sky Survey (2MASS). The original sample observed by IUE was trimmed to remove stars with poorer data, unreddened stars, and unusual stars (Be stars, luminosity class I stars, and early/luminous O stars), leaving 328 stars in the main FM07 sample.

FM07 introduced an “extinction-without-standards” technique in which they determine extinction based on a best-fit model SED for the observed flux from each star. This model-based method eliminates the need for observations of unreddened comparison stars (the pair method). The accuracy of the pair method can be affected by spectral mismatch between the target and

comparison star. Furthermore, the comparison stars themselves are not entirely dust free and require an extinction correction.

FM07 published the extinction curves in parameterized form, using a parameterization that is an expanded version of the one given in Fitzpatrick & Massa (1990). In particular, for the UV region ($\lambda < 2700 \text{ \AA}$), they use

$$k(\lambda-V) = \begin{cases} c_1 + c_2x + c_3D(x, x_0, \gamma) & x \leq c_5, \\ c_1 + c_2x + c_3D(x, x_0, \gamma) + c_4(x - c_5)^2 & x > c_5 \end{cases} \quad (1)$$

where $x \equiv \lambda^{-1}$, with λ in μm . In Fitzpatrick & Massa (1990), c_5 was fixed at $5.9 \mu\text{m}^{-1}$, whereas most values determined through the new parameterization are in that vicinity. $D(x, x_0, \gamma)$ represents the 2175 \AA bump, and is expressed using the Lorentzian-like function

$$D(x, x_0, \gamma) = \frac{x^2}{(x^2 - x_0^2)^2 + x^2\gamma^2}. \quad (2)$$

where x_0 specifies the location of the bump and γ modulates its width.

To describe the optical and near-IR portions of the extinction curve, FM07 employ a cubic spline interpolation. In the optical range, interpolation is based on extinction at $3300, 4000, \text{ and } 5530 \text{ \AA}$. In the near-IR ($\lambda > 1 \mu\text{m}$), FM07 assume that the extinction curve is universal (i.e., $A_\lambda/A_{1\mu\text{m}} = \text{constant}$ when $\lambda > 1 \mu\text{m}$, for all stars) and follows the generally assumed power-law functional form (Rieke & Lebofsky 1985):

$$A_\lambda \propto \lambda^{-\beta_{\text{NIR}}} \quad (3)$$

with the exponent $\beta_{\text{NIR}} = 1.84$ (Martin & Whittet 1990). Assuming a fixed near-IR curve was justified in FM07 due to the use of relatively shallow *JHK* data from 2MASS. Fitzpatrick & Massa (2009) added new spectral observations from HST's Advanced Camera for Surveys High Resolution Camera to investigate the potential for flexibility in the near-IR power law slope. They demonstrate that, of the 14 stars studied, over half of the NIR power-law fits are significantly improved by allowing β_{NIR} to be a free parameter. They show specifically that the use of fixed $\beta_{\text{NIR}} = 1.84$ from Martin & Whittet (1990) is not a good fit for large- R_V sightlines. Furthermore, the slope appears to be correlated with R_V . Considering that there is still some debate in the literature concerning the nature of IR extinction, we produce two sets of extinction curves. One follows FM07, with a universal extinction curve at $\lambda > 1 \mu\text{m}$. The other follows FM07 up to 7500 \AA , but subsequently follows a power-law parameterization with a variable exponent β_{NIR} . The wavelength at which the regime changes is

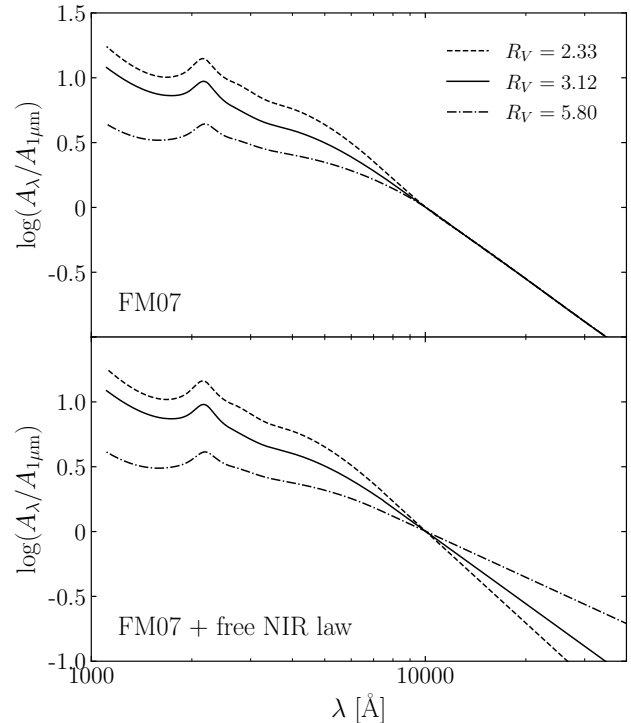


Figure 1. An illustration of the two sets of extinction curves that will be explored in this work, using stars from our sample with R_V values of 2.33, 2.12, and 5.80. *Top:* Curves produced by the FM07 parameterization in which the near-IR extinction curve has a fixed (universal) slope. *Bottom:* Same as above for $\lambda < 7500 \text{ \AA}$, but allowing the near-IR extinction curve slope to be free (i.e., R_V -dependent) as described in Section 2.1. Note that the curves are normalized at $1 \mu\text{m}$ in order to show the fixed curve assumed in FM07. Also, the curves are shown in log scale, again to highlight the difference in the near-IR.

based on the analysis in Fitzpatrick & Massa (2009). The exponent for each sightline is determined according to the relation in Salim & Narayanan (2020) constructed from the data reported in Table 3 of Fitzpatrick & Massa (2009):

$$\beta_{\text{NIR}} = -4.20 + 4.59 \left(\frac{A_B}{A_V} \right), \quad (4)$$

where $A_B/A_V \equiv 1 + 1/R_V$. In other words, the near-IR exponent inversely depends on R_V . The two sets of extinction laws are illustrated in Figure 1 for three stars from the FM07 sample with a range of R_V values. Note that the extinction curves with non-universal β_{NIR} show no break in slope around 7500 \AA , even though this transition is not smooth by construction; they appear more natural.

We use extinction curves from Gordon et al. (2003) for sightlines to SMC stars. The authors fit reddened stars from both the SMC (wing and bar sample stars)

and the LMC (LMC2 supershell and normal samples) to the parameterization in [Fitzpatrick & Massa \(1990\)](#).

2.2. Column densities

To obtain hydrogen column density measurements, we use the database of literature values for 3008 sightlines to stars compiled in [G12](#). [G12](#) contains two tables: one with all of the measurements found in the literature, and a second with only the most recent measurements for each sightline. We use the latter. [G12](#) reports $N(\text{H I})$ and $N(\text{H}_2)$, along with an $N(\text{H})$ entry, meaning $N(\text{H I} + \text{H}_2)$. It is notable that these $N(\text{H I} + \text{H}_2)$ values sometimes differ somewhat from the combination of individual density values ($= N(\text{H I}) + 2N(\text{H}_2)$). This is due to the disparate sources from which information was obtained, and the fact that individual $N(\text{H}_2)$ and $N(\text{H I})$ measurements have sometimes been reported in the literature more recently than $N(\text{H})$ for the same sightline. For relative consistency, we use the $N(\text{H})$ column as opposed to the summed individual values, and refer to it as $N(\text{H I} + \text{H}_2)$ or $N(\text{H})$ interchangeably.

Some column density values do not have associated errors, in which case we adopt the mean of the log-errors on the density measurements with reported errors. The notable exception is the sightline toward HD 149757 (ζ Oph), which had an error value on $N(\text{H})$ that was over an order of magnitude smaller than all the others, and therefore appears erroneous. We reset the error value for this star to the average (as if it did not originally have one).

[G12](#) includes column density measurements for a great many species, of which we use $N(\text{Fe II})$, $N(\text{O I})$, $N(\text{O VI})$, $N(\text{Mg II})$, and $N(\text{Ca II})$. We pull updated hydrogen column densities for SMC stars from [Welty et al. \(2012\)](#)¹, which was published after the [G12](#) compilation.

The lines used to determine column densities for the species in question lie in the UV (except for the Ca II H and K lines), necessitating the use of data from space-based instruments such as *IUE*, *FUSE*, STIS on *HST*, etc.

2.3. Sample selection

We matched the 328 stars with extinction curves from [FM07](#) to the list of 3008 stars with column density measurements from [G12](#) by matching the stars by name. The [FM07](#) stars are mostly $V < 10$ mag, with a few slightly fainter; this means the stars all have names from common catalogs. Ninety-six stars are common to [FM07](#) and [G12](#), of which 70 stars have $N(\text{H I})$ measurements,

54 have $N(\text{H}_2)$ measurements, and 50 have $N(\text{H I} + \text{H}_2)$ reported. For some stars in the [FM07](#) sample, R_V was assumed to be 3.1 because of a lack of IR photometry. For others, the O_1 spline point was not calculated due to missing *U*-band photometry. We omit stars which fit within either category. This leaves us with 41 sightlines in the $N(\text{H})$ sample and 55 in the $N(\text{H I})$ -only sample.

Pertaining to the analysis of metallicity effects in [Section 3.3](#), of the 41 stars in the $N(\text{H I} + \text{H}_2)$ sample, 28, 27, 9, 21, and 23 stars have Fe II, O I, O VI, Mg II, and Ca II, respectively.

For the SMC analysis in [Section 4.3](#), we first matched the five reddened SMC stars from [Gordon et al. \(2003\)](#)—four bar sample stars and one from the wing sample—with the full [G12](#) list (again using names, as they all have AzV designations). Of the metal species of interest, only Ca II had column densities reported (for all but one star, AzV 23). [Welty et al. \(2012\)](#) includes $N(\text{H})$ measurements for all five stars. Notably, for AzV 23, AzV 214, and AzV 398 (all from bar sample), [Welty et al. \(2012\)](#) determined that there is no significant contribution to $N(\text{H})$ from $N(\text{H}_2)$.

3. RESULTS

The main objective of our analysis is to find the wavelength at which the hydrogen column density $N(\text{H})$ is best correlated with the extinction A_λ , which will reveal the best measure for the dust column in the Milky Way. In previous studies, either $E(B - V)$ or A_V has been taken as the measure for dust simply because those measures are most widely available. Furthermore, in many cases where A_V is used, it has simply been obtained through $A_V = 3.1E(B - V)$, i.e., assuming a fixed extinction curve. However, the literature also hints that the true measure of dust may be found somewhere in the NIR (e.g., [Jura 1980](#); [Schlafly et al. 2016](#)), though this has not been verified. As our analysis covers wavelengths from the far UV to *K* band in the NIR, we are able to assess different possibilities.

It is also noteworthy that previous studies have uniformly assumed linearity in the relation between $N(\text{H})$ and $E(B - V)$ or A_V . In the case of diverse extinction curves (a range of R_V), we do expect linearity with respect to the A_λ that is the true measure of dust (which may or may not be A_V), but not at other wavelengths. Instead of assuming linearity, we allow a power-law dependence of $N(\text{H I})$ and $N(\text{H I} + \text{H}_2)$ on A_λ (and $E(B - V)$).

3.1. $N(\text{H I} + \text{H}_2)$

Using the [FM07](#) extinction curve parameters for our sample of 41 sightlines, we calculate for each reddened

¹ Obtained from the full data table at <https://astro.uchicago.edu/~dwelty/mcoptuv.html>.

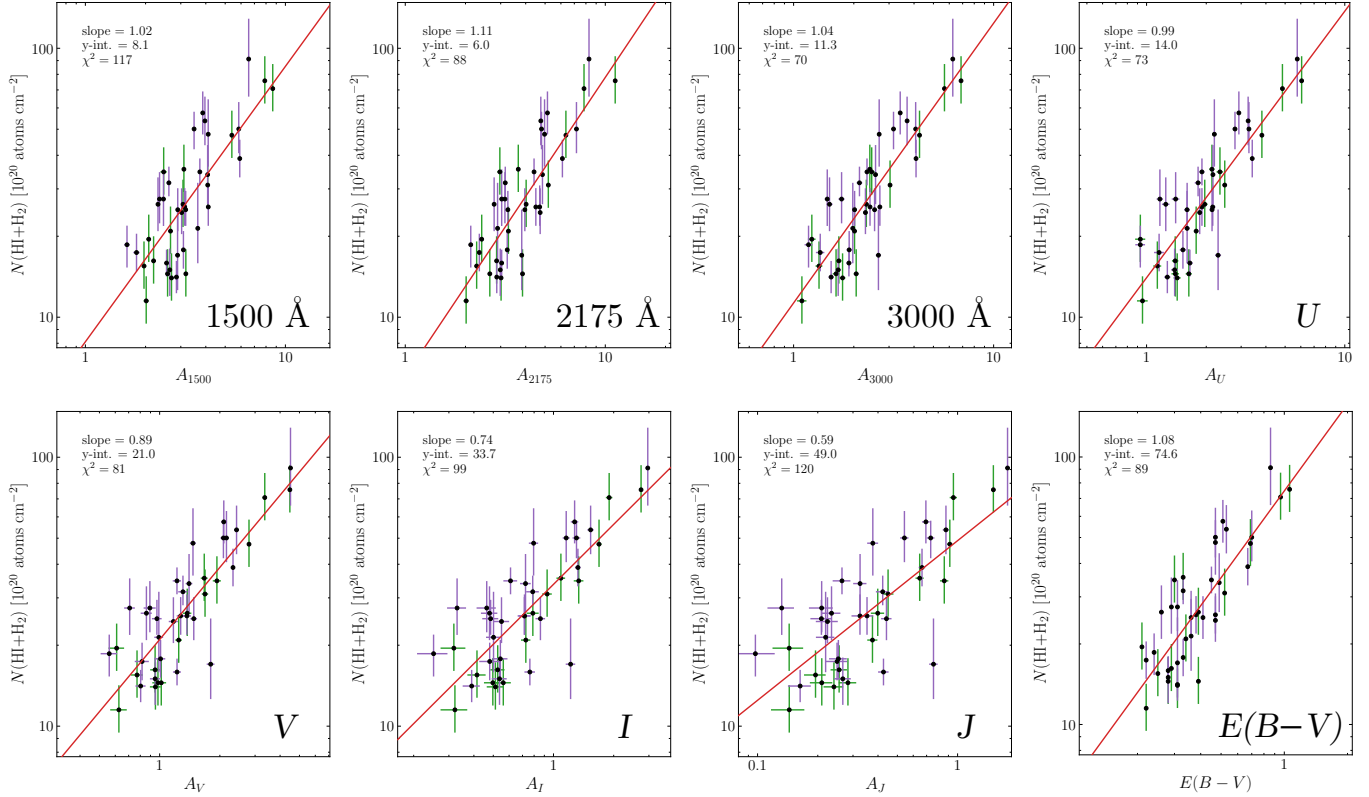


Figure 2. Relationship between total hydrogen column density and extinction at 7 selected wavelengths, along with the standard $N(\text{H I} + \text{H}_2)$ vs. $E(B - V)$ for comparison. Where the name of a photometric band is used, λ is the standard central wavelength of the filter. Points with green errorbars are those without $N(\text{H I} + \text{H}_2)$ errors reported in G12, treated as described in Section 2.2. Points with purple errorbars had errors reported. In each plot, the two relevant parameters corresponding to Equation 5 are reported in the upper left. Values for y -intercepts are reported in units consistent with the plot axis. χ^2 values from the fits to Equation 5 are also reported. The fit is best in the 3000 Å panel. There are 39 degrees of freedom for all fits.

star the extinction (A_λ) for wavelengths in the range 1111 Å to 47000 Å, pseudo-continuously sampling 1000 wavelengths from the range logarithmically. Extinctions are calculated using a modified version of the fm07 function from the `extinction` package in Python (Barbary 2016). We adjust the function such that it can use arbitrary curve parameters and any R_V . Uncertainty on the resultant A_λ values is calculated by re-running the script with modified R_V values, once using $R_V + \sigma_{R_V}$, and again using $R_V - \sigma_{R_V}$ (where σ_{R_V} is provided in FM07). The resulting range of A_λ for each star should be a good approximation of the uncertainty, since the error is dominated by σ_{R_V} . After the first run, we also calculated a second set of extinction curves, this time with R_V -dependent β_{NIR} redward of 7500 Å.

Figure 2 shows a selection of wavelengths for which $N(\text{H I} + \text{H}_2)$ is plotted against A_λ : the UV wavelengths 1500 Å, 2175 Å, 3000 Å, along with the approximate central wavelengths of the standard photometric bands U (3700 Å), V (5500 Å), I (8000 Å), and J (1.2 μm). The final panel shows $E(B - V)$ in place of extinction at

a specific wavelength. Values for A_I and A_J are based on extinction curves with free β_{NIR} . Also shown are best power-law fits calculated using the least-squares method:

$$\log N(\text{H I} + \text{H}_2) = a \log A_\lambda + b, \quad (5)$$

where $a = 1$ would correspond to a linear relation between $N(\text{H I} + \text{H}_2)$ and A_λ (in that case, b gives the gas-to-dust ratio assuming A_λ as the dust measure). Errors on $N(\text{H I} + \text{H}_2)$ from G12 are taken into account in the fit. We calculate a χ^2 value for each individual fit, which is to first order proportional to the scatter of the residuals around the best fit.

Following the original formulation from Bohlin et al. (1978), most studies assume a linear relation, typically with $A_\lambda = A_V$, or using $E(B - V)$ as the independent parameter. From Figure 2 we conclude that neither option is optimal. The scatter (χ^2) is smaller in the UV and blue optical than at longer wavelengths. Also, the relation is closer to linear in the UV and blue optical than at longer wavelengths (including near-IR). The relation

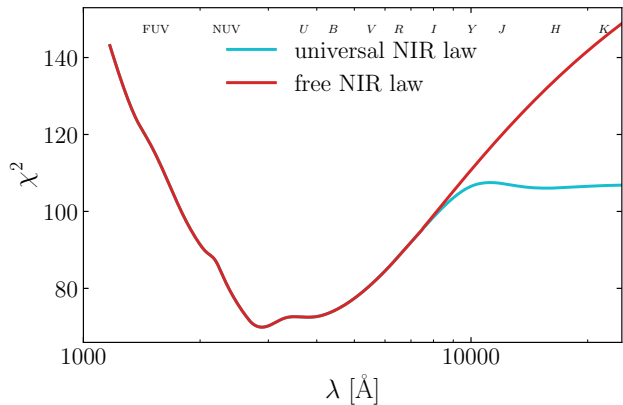


Figure 3. The sum of normalized quadratic residuals (χ^2) between $\log N(\text{H I} + \text{H}_2)$ and $\log A_\lambda$ as a function of wavelength. The χ^2 value comes from a fit to Equation 5. There are 39 degrees of freedom. The cyan curve represents fits done using A_λ values calculated using the original, unadjusted FM07 extinction curve parameterization. The red curve is the same at $\lambda < 7500$ Å, but above that wavelength, A_λ is adjusted from the FM07-calculated values using an R_V -dependent near-IR extinction curve slope (β_{NIR} ; see Section 2.1). The relation between $N(\text{H I} + \text{H}_2)$ and extinction is tightest for extinction around 2900 Å. Letters representing common photometric bands are centered on their central wavelengths.

against $E(B - V)$ is similar in quality to the relation in V band and likewise is not quite linear. The inferiority of near-IR extinction as a measure of dust would also hold using a fixed NIR law, since it already sets in at A_I (~ 8000 Å).

In Figures 3 and 4, we look at the χ^2 and the slope of the best fit at continuous wavelengths instead of wavelengths corresponding to specific bands. Results are shown for both the universal (cyan) and free (red) NIR curves. We show in Figure 3 that there is a wavelength region where the scatter is minimized lying in the near-UV and blue optical. Specifically, the correlation is best at $\lambda \approx 2900$ Å, with $\chi_{\text{red}}^2 = 1.8$. This lends itself to the notion that total hydrogen column density is most closely related to dust extinction at or around that wavelength, and therefore that A_{2900} is the best measure of the dust column density in the Milky Way.

To derive the error on the best-fit wavelength, we perform a bootstrapping procedure by taking 1000 random samples with replacement. We fit a Gaussian to the histogram of wavelengths where χ^2 was lowest, restricted to the 2000 to 4000 Å regime, since the distribution had high-wavelength outliers. The standard deviation of that Gaussian, and therefore the error on the best-fit wavelength, is 160 Å. The best-fit wavelength is therefore relatively well-constrained by our data.

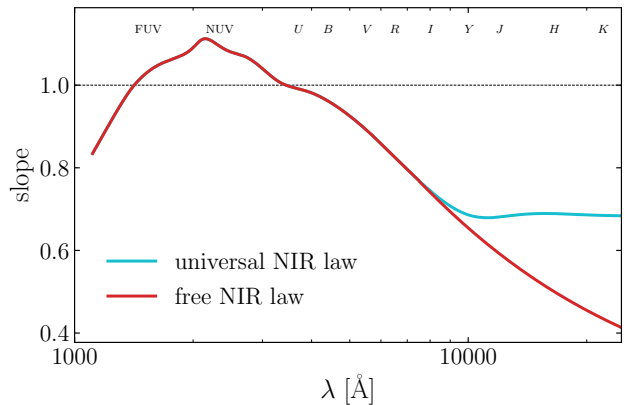


Figure 4. Slope (a from Equation 5) between $\log N(\text{H I} + \text{H}_2)$ and $\log A_\lambda$ as a function of wavelength. The cyan curve represents fits done using A_λ values calculated using the original, unadjusted FM07 extinction curve parameterization. The dotted line represents a slope of 1 (a linear relationship between total hydrogen column density and extinction). The relation between $N(\text{H I} + \text{H}_2)$ and extinction is exactly linear for extinction around 3000 Å.

It is commonly assumed that the slope of the $N(\text{H})$ vs. $E(B - V)$ relation is 1, and therefore that the slope is also 1 for $N(\text{H})$ vs. A_V if the extinction curve does not change from star to star. Our analysis casts these assumptions in a new light. For the $E(B - V)$ relation, we find the slope to be 1.08 (with $\chi_{\text{red}}^2 = 2.3$), implying possible nonlinearity, but in general agreement with the oft-assumed 1. For A_V , we find the slope to be 0.89 ($\chi_{\text{red}}^2 = 2.1$), again close to linear but not exactly so. Using a similar bootstrapping method to the one described above, we find the wavelength where the relation is exactly linear to be in the region of 3000 Å, with error 300 Å. This value agrees within errors with the 2900 ± 160 Å which we find for the best fit. The agreement confirms that the relation *is* linear between $N(\text{H})$ and the best dust measure—which is A_{2900} instead of A_V or $E(B - V)$.

For reference, the best fits are as follows:

$$\log N(\text{H I} + \text{H}_2) = 1.05 \log A_{2900} + 21.03 \quad (6)$$

$$= 0.89 \log A_V + 21.32 \quad (7)$$

$$= 1.08 \log E(B - V) + 21.87 \quad (8)$$

where the free coefficient b represents the logarithm of hydrogen column density at A_{2900} , A_V , or $E(B - V)$ of 1. The error on $N(\text{H})$ determined from these expressions is ~ 0.03 dex (7%), and is obtained by taking the typical error in $N(\text{H})$ measurements of 0.1 dex, scaling it by χ_{red}^2 (~ 2), and dividing it by the square root of the sample size, resulting in the error of the mean. When compared at $E(B - V)$ (or A_V) values appropriate for

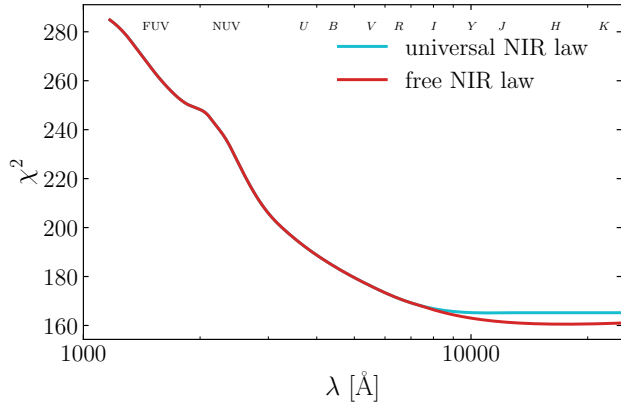


Figure 5. The sum of normalized quadratic residuals (χ^2) between $\log N(\text{H I})$ and $\log A_\lambda$ as a function of wavelength. The χ^2 value comes from a fit to Equation 5. There are 53 degrees of freedom. The cyan curve represents fits done using A_λ values calculated using the original, unadjusted FM07 extinction curve parameterization. The relation between $N(\text{H I})$ and extinction is tightest for extinction around $1.7 \mu\text{m}$, but is much less tight than for $N(\text{H I} + \text{H}_2)$.

the respective samples, the $N(\text{H})$ from our expressions is 10% higher than the value from Bohlin et al. (1978), 6% higher than the value from G12, and 8% lower than the value derived in Zhu et al. (2017) from their analysis of the whole Anders & Grevesse (1989) sample. These differences are well within the range of statistical error. The advantage of using our nonlinear expressions is that they acknowledge that gas-to-dust ratio is not exactly a constant, especially when $E(B - V)$ or A_V is used to measure the dust.

The sightlines used in this study span the reddening range $0.21 < E(B - V) < 1.06$, with a median value of 0.36 for the $N(\text{H I} + \text{H}_2)$ sample and 0.33 for the $N(\text{H I})$ sample. At $E(B - V) \approx 0.08$, there is a well-known break in the slope of the $N(\text{H})$ vs. A_λ relation (e.g., Savage et al. 1977; Bohlin et al. 1978; Liszt 2014). This can be attributed to H_2 formation on the surface of dust grains (Hollenbach & Salpeter 1971), which only begins in regions characterized by sufficiently large reddening values (i.e., denser regions). Because we do not probe below $E(B - V) = 0.2$, we are not sensitive to this change in slope and do not discuss it further.

3.2. $N(\text{H I})$ only

We carry out the same analysis as above, but using $N(\text{H I})$ instead of $N(\text{H I} + \text{H}_2)$. Since $N(\text{H I})$ measurements along Galactic sightlines are more abundant in the literature than those for $N(\text{H}_2)$, we are able to include 55 sightlines here. It is well-established that the overall correlation with $E(B - V)$ and A_V is stronger when using $N(\text{H I} + \text{H}_2)$ (e.g., Bohlin et al. 1978; Welty et al.

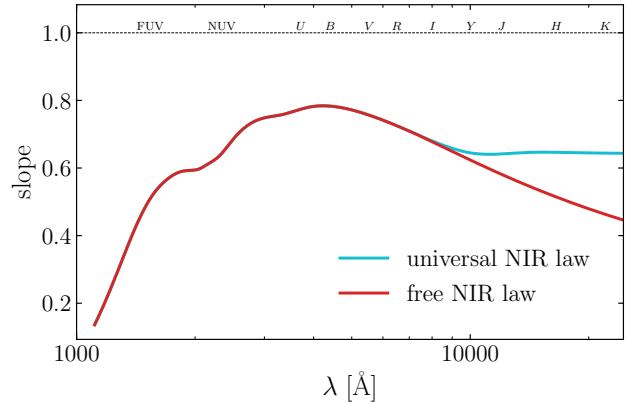


Figure 6. Slope (a from Equation 5) between $\log N(\text{H I})$ and $\log A_\lambda$ as a function of wavelength. The cyan curve represents fits done using A_λ values calculated using the original, unadjusted FM07 extinction curve parameterization. The dotted line represents a slope of 1 (a linear relationship between total hydrogen column density and extinction). The relation between $N(\text{H I})$ and extinction does not approach linearity.

2012). In comparing Figure 5, which shows χ^2 values for the fit between $\log N(\text{H I})$ and $\log A_\lambda$, with the corresponding Figure 3 for $N(\text{H I} + \text{H}_2)$, one can see that we reproduce the poorer fits. At V , $N(\text{H I} + \text{H}_2)$ produces $\chi_{\text{red}}^2 \approx 2.1$, whereas $N(\text{H I})$ produces $\chi_{\text{red}}^2 \approx 3.4$. The $E(B - V)$ fit is actually significantly worse for $N(\text{H I})$, with $\chi_{\text{red}}^2 \approx 4.6$ as opposed to $\chi_{\text{red}}^2 \approx 2.3$ for $N(\text{H I} + \text{H}_2)$.

It is noteworthy that for $N(\text{H I})$ the best fit does not lie in the visible range; rather, the fits gradually improve toward in the NIR, stabilizing beyond about $1 \mu\text{m}$ (see Figure 5). We concluded in Section 3.1 that a minimum value exists at $\lambda \approx 2900 \text{ \AA}$, but $N(\text{H I})$ does not seem to be connected to the dust in the same way, as expected given that H_2 is known to form on the surface of grains. In Figure 6, we see that the relation never approaches linearity, again contrasting with the $N(\text{H I} + \text{H}_2)$ case. This behavior can be attributed to the fact that we are not counting all of the hydrogen.

3.3. Metallicity effects on the gas-to-dust ratio

Though $N(\text{H I} + \text{H}_2)$ is strongly correlated with A_λ , especially in the near-UV/blue optical, χ_{red}^2 is not 1, indicating excess scatter not described by the errors. Excess scatter has been a consistent feature of such relations in the literature with $E(B - V)$ and A_V used to represent the dust, but even at A_{2900} (which we claim is the true best dust measure, and therefore any scatter due to differences in the extinction curve is minimized; see Section 4), the errors on $N(\text{H I} + \text{H}_2)$ do not encapsulate the scatter. A leading possibility for the residual scatter is variation in metallicity (e.g., Welty et al. 2012;

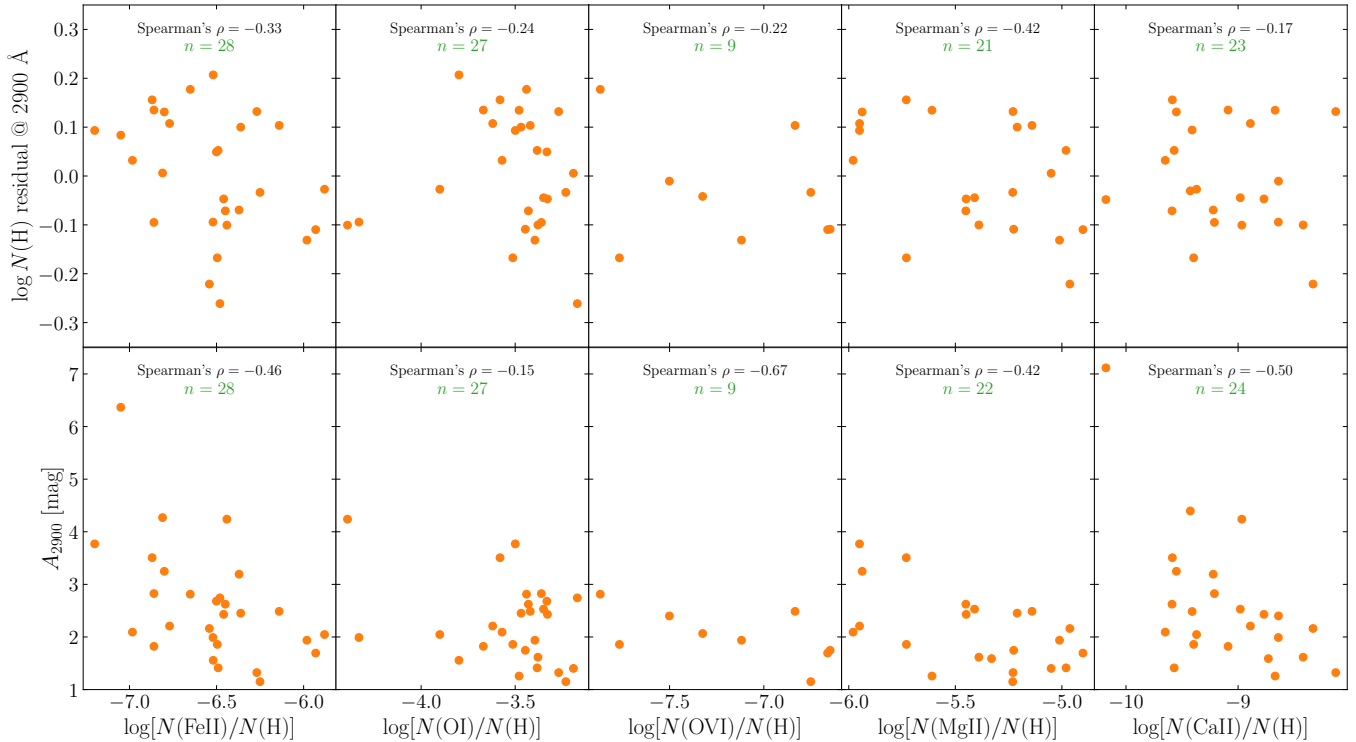


Figure 7. Metallicity, gas-to-dust ratio, and depletion of metals onto dust grains. *Top:* The dependence of the residuals in the $N(\text{H I} + \text{H}_2)$ vs A_λ relation (i.e. gas-to-dust ratio) on metallicity, which is represented by the column density of five different metals normalized by the total hydrogen density. *Bottom:* Extinction at A_{2900} (our preferred measure of dust) vs. the column density of metals. The Spearman correlation coefficient is given in each panel, along with the total number of sightlines with a column density for the given species reported in G12. While the correlations are mostly quite weak and some are not statistically significant, they are all in the negative direction, which is what we expect if the higher *cosmic* abundance (which the *observed* abundances shown reflect only partially) are related to higher gas-to-dust ratio (upper panels) and if the higher *observed* abundances correspond to less depleted sightlines (i.e., lower extinction; lower panels).

Rémy-Ruyer et al. 2014; Kahre et al. 2018). If one accounts for differing metallicity between sightlines, it may be possible to bring the χ_{red}^2 nearer to unity.

We make use of common metallicity indicators (Fe II, O I, O VI, Mg II, and Ca II) in the G12 compilation to assess metallicity effects among the sightlines toward our stars. To test whether metallicity is in fact correlated with residuals (thus driving the scatter), we plot the residual at $\lambda = 2900 \text{ \AA}$ from Section 3.1 (essentially the gas-to-dust ratio) vs. the column density of the metal species, normalized by $N(\text{H I} + \text{H}_2)$.

The results are shown in the top row of Figure 7. We also provide Spearman's rank correlation coefficient ($-1 < \rho < 1$) in each panel, which assesses the correlation nonparametrically (i.e., does not assume linearity). Though most correlations are weak or nonexistent, it is significant that all values of Spearman's ρ are negative, implying that a very weak correlation with metal densities is not ruled out.

The inability of the metallicity to account for the scatter in the gas-to-dust relation, even when dust is measured as A_{2900} , may seem disappointing. However, it is not clear that one can use the *observed* metal abundances alone to test the hypothesis in the first place. In fact, many metal species are subject to depletion onto dust grains themselves, so that the gas-phase abundances we measure towards these stars do not represent the true “cosmic” abundance along any given sightline. For Si in particular, depletion is known to essentially entirely offset the observed gas metallicity differences among the Milky Way and the Magellanic Clouds (Roman-Duval et al. 2019). In the ISM, among the species we investigate, Fe and Ca are likely substantially depleted, with the Ca depletion depending more strongly on gas density; Mg is largely undepleted in diffuse gas but depleted in denser gas; and O is not strongly depleted (all inferences from Mathis 1990). If depletion (rather than the intrinsic range of cosmic abundances) is indeed the principal cause of the observed gas metal-

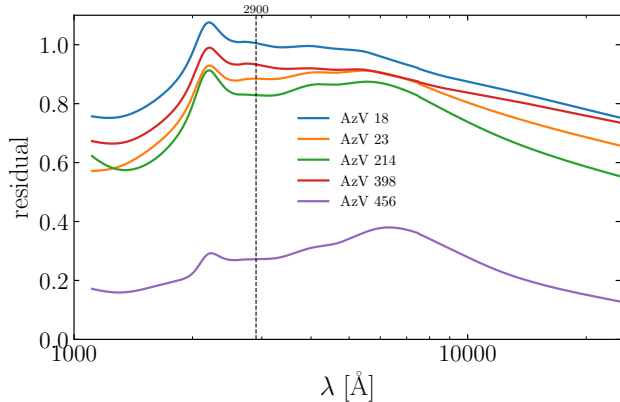


Figure 8. Residuals of $\log N(\text{H I} + \text{H}_2)$ of SMC stars from Gordon et al. (2003) with respect to $\log N(\text{H I} + \text{H}_2)$ for MW sightlines from the UV to the near-IR. The dashed vertical line represents the best-fit wavelength from Section 3.1 ($=2900 \text{ \AA}$).

licity differences between sightlines, there should exist a correlation between depletion and dust density, which may be reflected in a correlation between the observed metallicity and extinction. In the bottom five panels of Figure 7, we show extinction vs. observed metallicities. For Fe II and Ca II, there is a relatively clear negative correlation between A_{2900} and normalized column density—the more dust there is, the more the metals are depleted onto it. The correlation is somewhat weaker but still present for Mg II, which aligns again with Mathis (1990). The two O species seem to be subject to relatively little depletion, though still have weak negative gradients. Connecting the lower panels with those in the top, it appears that it is not possible to assess the metallicity effects on the gas-to-dust ratio within the Milky Way.

3.4. SMC

So far we have focused only on the Milky Way. In the context of hydrogen column density vs. extinction/reddening, the SMC has relatively low $E(B - V)$, but high $N(\text{H I} + \text{H}_2)$. This would place most SMC sightlines in the upper-left region of the $N(\text{H I} + \text{H}_2)$ vs. $E(B - V)$ panel in Figure 2, far above the MW best-fit line. To quantify the deviation, we pull the 5 SMC stars for which Gordon et al. (2003) derived a full extinction curve, four from the bar sample, and one from the wing sample. The wing sample shows extinction features much more similar to the MW than the bar does, which Gordon & Clayton (1998) propose is a result of weaker star formation in the wing region. It has been suggested that the strong positive offset (for the bar sample especially) is due to the lower-metallicity environment in the

SMC (e.g., Welty et al. 2012; Rémy-Ruyer et al. 2014). We find this offset to be 0.9 dex when $E(B - V)$ is used as the measure of dust. The question we wish to answer here is how much of the offset may be the result of not measuring the dust using a more adequate tracer.

Figure 8 shows the residuals of SMC sightlines with respect to the $N(\text{H I} + \text{H}_2)$ vs A_λ relations for MW sightlines carried out in Section 3.1. The plot confirms the large offsets in the optical region (around V band), especially for the bar sample stars. However, the offsets are clearly reduced in the UV, albeit at wavelengths shorter than 3000 \AA . This lends more evidence toward our conclusion from Section 3.1 that dust is better measured using extinctions at UV wavelengths. We discuss a possible framework for bringing the MW and SMC gas-to-dust ratios into full agreement in Section 4.3.

4. DISCUSSION

4.1. A physically motivated measure of the dust column for the Milky Way

Through studying the correlation between $N(\text{H})$ and A_λ from the UV to the NIR, we find that the extinction at 2900 \AA (A_{2900}) is more fundamental than $E(B - V)$ or A_V as a measure of dust, at least for the MW. Further, the slope of the relation is equivalent to unity around this wavelength, solidifying the result.

Does this result have any theoretical basis? As we pointed out in the introduction, Kim & Martin (1996) mention that $A_V/N(\text{H})$ is not necessarily the best measure of the dust to gas mass ratio. Half a century ago, Purcell (1969) suggested an alternative to $A_V/N(\text{H})$ based on the application of the Kramers-Kronig relations to the interstellar medium. For a single grain composition, the integral relation can be derived from the original Kramers-Kronig expressions (Purcell 1969; Martin 1978; Bohren & Huffman 1983). The idea is to integrate the total extinction cross-section of the grains across all wavelengths, by integration of the extinction curve A_λ (or A_w , where $w \equiv \lambda^{-1}$):

$$\int_0^\infty \frac{A_w}{N(\text{H})w} d \ln w = 1.086\pi^2 m_{\text{H}} \sum \frac{f}{s_d} \frac{M_d}{M_{\text{H}}}. \quad (9)$$

Here, s_d is grain density (which depends on composition), and M_d is the column mass density of dust corresponding to hydrogen column mass density $M_{\text{H}} = m_{\text{H}}N_{\text{H}}$.

Kim & Martin (1996) plot the integrand from Equation 9 for a combination of silicate and graphite grains, with separate curves for extinction curves with varying values of R_V . The authors point out that all curves cross near $2.8 \mu\text{m}^{-1}$ (3600 \AA). This point of invariance of gas-to-dust mass ratios with R_V coincides roughly with our

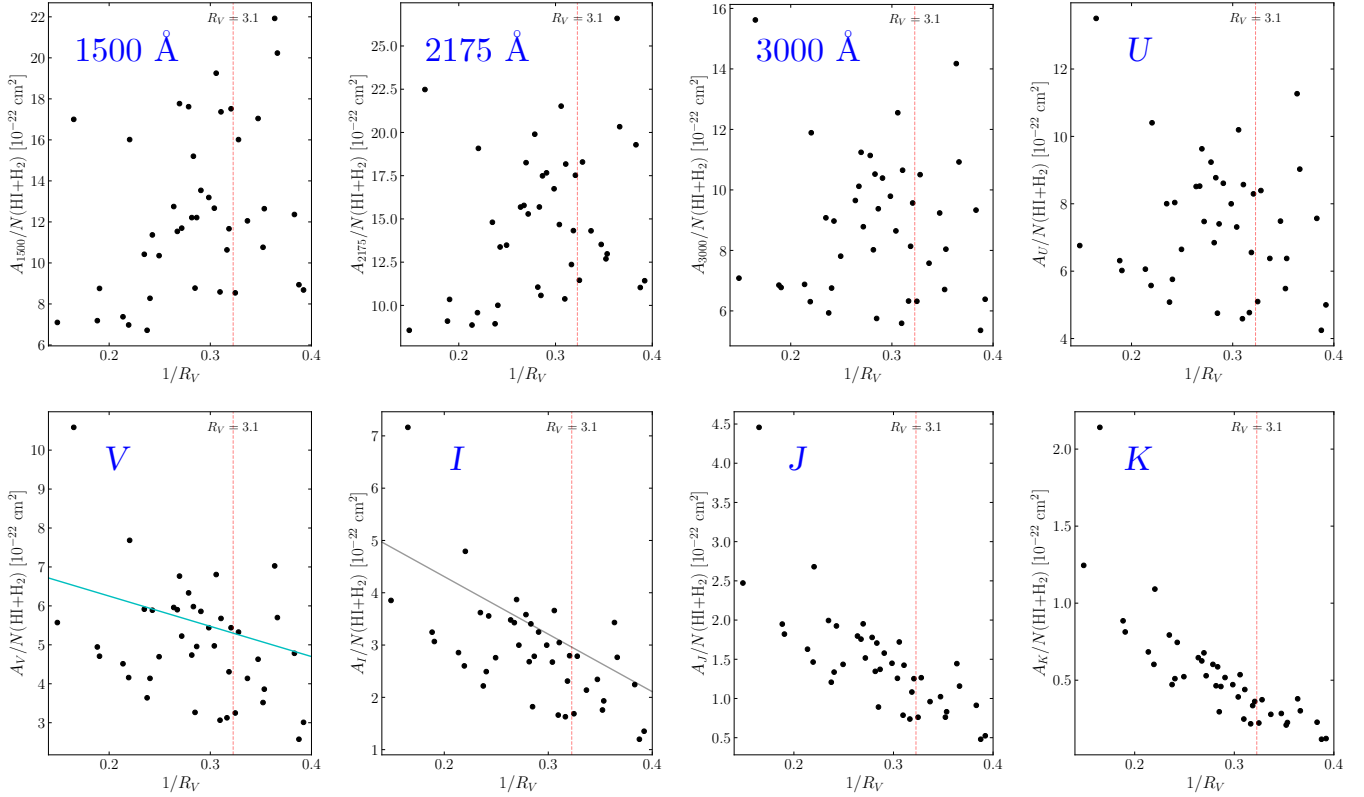


Figure 9. Dust-to-gas ratio for 41 individual sightlines vs. $1/R_V$, where the dust is represented by extinction at specific wavelengths from the UV to the NIR, as indicated by the labels. Vertical dashed line indicates where $R_V = 3.1$, for convenience. Note that y -axis ranges vary. For the last three panels (I , J , K), the extinction values are derived using the variable NIR extinction curve slope (β_{NIR} ; see Section 2.1). The cyan line on the A_V panel represents predictions from Kim & Martin (1996). The A_I panel is analogous to Figure 2 from Draine (2003), and the gray line represents the best fit from that plot. Dust-to-gas ratio is independent from R_V at 3000 Å and at U , confirming the results obtained earlier in this work.

best- χ^2 wavelength of 2900 Å from Section 3.1. While these results do not coincide precisely, their separation is not large considering the modest increase in our χ^2 value from 2900 Å to 3600 Å (see Figure 3). The Kim & Martin (1996) result is also in general agreement with the place we find the slope of the $N(\text{H})/A_\lambda$ relation to be 1 ($\sim 3000 \pm 300$ Å). Referencing Figure 4, one can see that the crossing point we find without bootstrapping is quite close to the U -band, which is centered very nearby 3600 Å.

In a similarly mass-based pursuit, Barbaro et al. (2004) select lines of sight in the solar neighborhood with anomalously high $N(\text{H I})/E(B - V)$. They find that the mass density ratio of gas to dust ($\rho_{\text{H}}/\rho_{\text{d}}$) is linearly related to $N(\text{H})/E(B - V)$, which demonstrates that $E(B - V)$ cannot be the fundamental measure of dust, as we also find. They also note that, for anomalous sightlines, a modification of $\rho_{\text{H}}/\rho_{\text{d}}$ compared with the Galactic standard is required.

As the above analysis based on the Kramers-Kronig approach also demonstrates, if some A_λ is truly the

best measure of dust, we expect the gas-to-“dust” ratio (where the extinction A_λ represents dust) to be independent of R_V . We perform a test for R_V dependence across all wavelengths probed in the main analysis (UV to NIR), and show a selection of wavelengths in Figure 9. Figure 9 shows the wavelength regime where $A_\lambda/N(\text{H})$ is independent of R_V : somewhere around 3000 Å or U band. This agrees with our result obtained using a different method (minimization of scatter between $N(\text{H})$ and A_λ). While the switch from slight positive to slight negative correlations in the plots is subtle, it is clear that at A_V and beyond, there is a definite relationship between $A_\lambda/N(\text{H})$ and R_V , providing more evidence for ruling out extinction at those wavelengths as a satisfactory dust measure. Kim & Martin (1996) found that as R_V increased beyond the standard 3.1, their maximum entropy solution did not use up as much material, yielding increased $A_V/N(\text{H})$. These predictions are shown in cyan on the V panel of Figure 9. Draine (2003) constructs an R_V -dependent relation for $A_I/N(\text{H})$, using 14 sightlines through translucent clouds from Rachford

et al. (2002). The resultant relation is shown in gray on the I panel of Figure 9. Both the Kim & Martin (1996) and Draine (2003) relations agree with what we find.

4.2. The character of the near-IR extinction curve

In our analysis, we have produced the near-IR parts of the extinction curves by two different methods: (1) assuming universality beyond $1 \mu\text{m}$ (following the FM07 parameterization that imposes it), and (2) modifying the FM07 parameterization beyond $0.75 \mu\text{m}$ in order to allow the NIR slope to vary with R_V , following the results from Fitzpatrick & Massa (2009). We see that our results are entirely unaffected by this assumption. The reason for considering NIR extinction as a more physically motivated measure lies in the notion that the NIR extinction curve may be universal (Rieke & Lebofsky 1985; Cardelli et al. 1989). A universal curve in the NIR means that the ratio of extinctions for any two wavelengths in the NIR range will be constant, even if the shape of the curve in the UV/optical is variable (and, following Cardelli et al. 1989, is correlated with R_V). However, the possibility that the NIR extinction curve is universal only guarantees that any NIR extinction (e.g., A_I , A_J , A_K) will be an equally good (or bad) measure of the dust, but not necessarily the best measure. In other words, the question of universality in the near-IR has no bearing on which extinction measure is most closely related to dust column density.

While shedding light on the question of the character of the near-IR extinction curve is not the goal of this paper, we overview the subject briefly. The foundational study Cardelli et al. (1989) finds that the IR data of the time was consistent with a single extinction law for $\lambda > 0.90 \mu\text{m}$, citing several contemporary studies (Jones & Hyland 1980; Koornneef 1983; Rieke & Lebofsky 1985; Smith 1987; Whittet 1992) and ultimately using the Rieke & Lebofsky (1985) curve as the basis for the β_{NIR} used in their parameterization, with a value of 1.61. More recently, with deeper NIR data available, higher values have been found: 1.95 (Wang & Jiang 2014), 2.07 (Wang & Chen 2019), and upward. Studies with the highest values (e.g., Naoi et al. 2007; Nogueras-Lara et al. 2018) focus on extremely dense regions (like the Galactic Center and the Coalsack). Steeper slopes may correlate with the density of the regions probed, pointing to non-universality. Indeed, it may be claimed that the wealth of recent works whose results span a wide range of β_{NIR} values themselves contribute to a variable β_{NIR} as a conglomerate.

As referenced in Section 2.1, the strongest case for non-universality may come from Fitzpatrick & Massa (2009). The resultant values for β_{NIR} varied from 0.9

to 2.3, and their Figure 3 reveals a correlation between near-IR slope and optical slope (and therefore R_V) for the 14 sightlines. Zasowski et al. (2009) shows general agreement with the Fitzpatrick & Massa (2009) result, citing a variance in β_{NIR} with Galactocentric radius which seems to be consistent with higher values being found toward the Galactic Center. Similarly, Schlafly et al. (2016) find that their extinctions derived using the standard crayon technique agree better with the Fitzpatrick & Massa (2009) modification of the FM07 curve than the FM07 curve itself. They fit extinction curves to their reddening vector measurements by computing dm_b/dA , where dA is a small variation in extinction about a typical APOGEE $E(B - V) = 0.65$, and m_b is the observed magnitude in some bandpass b . This is done for bandpasses in the optical (*grizy*) and the NIR (H , K , $W1$, $W2$). The resultant fit ($\chi^2 = 26$) for Fitzpatrick & Massa (2009) curves—the only ones tested which allowed β_{NIR} to vary—was quite a bit better than for prior curves more similar to FM07, the closest contender being Fitzpatrick (1999, $\chi^2 = 93$). We point out that Figures 1, 3, 4, and 6 do seem to suggest, but not prove, that a non-universal IR law is more natural because it provides a continuation of the trends seen at shorter wavelengths.

4.3. Dependence of the gas-to-dust ratio on metallicity and the SMC

In the landscape of plots showing $N(\text{H})$ vs. $E(B - V)$, there is always quite a bit of scatter. Bohlin et al. (1978), found this scatter to be $\sim 30\%$ about the mean. In later studies (such as Rachford et al. 2009), the scatter remains. In all cases, the scatter is larger than can be explained by the errors. In our analysis, the scatter has been partially mitigated by substituting A_{2900} as the measure of dust. However, the resultant χ_{red}^2 still exceeds unity. We attempted to invoke metallicity effects to explain this in Section 3.3, but as noted, the depletion of various species renders the analysis murky.

The gas-to-dust ratio is well studied in the literature, both in the Galaxy and beyond, and versus a range of other parameters. Using a variety of Galactic X-ray sources, Zhu et al. (2017) find no correlation between $N(\text{H})/A_V$ and hydrogen number density, Galactocentric radius, or distance from the Galactic plane, where the latter two were looked into as a way to explore potential dependence on metallicity. Our results suggest that probing the gas-to-dust ratio using A_V , where the residuals are also driven by differences in the extinction curve (Figure 9), dilutes any dependence on metallicity, likely leading to the null result. Vuong et al. (2003) also use Galactic X-ray sources to study the ratio, but in nearby

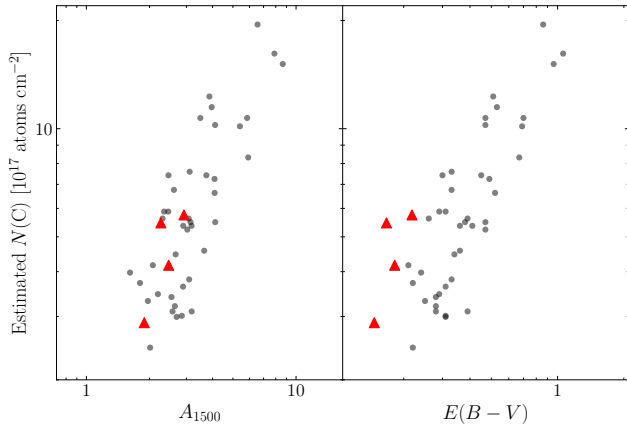


Figure 10. Estimated “cosmic” carbon column density for the 41 MW sightlines from Section 3.1 (gray points), overplotted with 4 sightlines to SMC bar sample stars from Gordon et al. (2003, red triangles), vs. extinction at 1500 Å (left) and $E(B - V)$ (right). $N(C)$ is estimated through adjusting the original $N(H)$ using constant shifts derived from $12 + \log(C/H)$ values for the MW (solar vicinity; Russell & Dopita 1992) or SMC (Toribio San Cipriano et al. 2017).

dense clouds, where the ratio (using A_J) in the ρ Oph cloud in particular is found to deviate significantly below the Galactic value. They extend this by finding that the difference between Galactic and local values for the ratio are entirely due to metallicity differences. Kahre et al. (2018) find a power-law relationship between the gas-to-dust ratio and gas-phase oxygen abundance measured from nebular emission in five nearby galaxies, along with a change in this relationship if H_2 is excluded from the gas tally. This result, based on *different* galaxies, is not necessarily in contradiction to our result—the lack of a strong correlation between gas-to-dust ratio and metallicity *within* our Galaxy, where the observed metallicity does not correspond to cosmic abundances as it does for global measurements based on H_2 regions.

In Section 3.4, we found that the difference in gas-to-dust ratio between the SMC and the MW using A_{1500} as the dust measure is smaller than using A_V or $E(B - V)$, but still persists. Interestingly, the remaining difference (~ 0.7 dex) matches the difference in the “cosmic” abundances of carbon between the Milky Way and the SMC (Russell & Dopita 1992; Clayton et al. 2000; Toribio San Cipriano et al. 2017), but not silicon (0.3 dex; Russell & Dopita 1992; Clayton et al. 2000). The relationship between differences in gas-to-dust ratio and differences in carbon abundance seems to be somewhat understood in the literature (Clayton & Martin 1985; Mathis 1990; Draine 2003; Welty et al. 2012), but exact agreement is achieved only when dust is measured using far-UV extinction (near UV is problematic because of the UV

bump; Figure 8). We illustrate the effects of switching to $N(C)$ in Figure 10, which shows the 4 bar-sample SMC sightlines from Gordon et al. (2003) overplotted onto two of the panels from Figure 2. In the right panel, it is clearly shown that the difference in cosmic abundance is *not* the sole factor in explaining the gas-to-dust ratio difference between the Milky Way and the SMC when one uses $E(B - V)$ to measure dust. However, the left panel shows that at 1500 Å, the difference in abundances *does* account for the disparity.

5. CONCLUSIONS

In this work, we set out to find the most fundamental measure of dust, and consequently of the dust to gas ratio. The main conclusions from this study are as follows.

1. The strongest correlation between total hydrogen column density $N(H\ I + H_2)$ and extinction A_λ for Milky Way sightlines is found at $\lambda \approx 2900$ Å; furthermore, the correlation is linear at that wavelength. A_{2900} is a superior measure of dust to $E(B - V)$ and A_V .
2. The result that A_{2900} is a more fundamental measure of dust supports a prediction by Kim & Martin (1996) through employment of the Kramers-Kronig relation for Milky Way dust. This approach also reveals that the wavelength of the extinction value which is the most physically motivated dust measure is grain size and grain composition specific, but generally lies in the UV.
3. We find no strong correlation between residuals from the $N(H\ I + H_2)$ vs. A_{2900} relation and metal column densities. However, we show that such an assessment of the drivers of the gas-to-dust ratio is not possible using the metallicities measured in the same sightlines as the reddened stars because of the depletion of metals onto dust grains. Indeed, we do see some evidence of depletion in the form of a correlation between A_{2900} and $N(\text{metal})/N(H)$.
4. The correlations between $N(H\ I)$ and A_λ are uniformly weaker than those for $N(H\ I + H_2)$, and are not linear for any A_λ .
5. The progression of the quality of the fits at longer wavelengths appears to proceed more naturally if we assume an R_V -dependent NIR extinction curve slope (β_{NIR}) than if we assume a fixed slope (i.e., a universal NIR curve).
6. Extinction at UV wavelengths also helps reduce the gap between the gas-to-dust ratios measured

for the SMC and the Milky Way. This difference is 0.9 dex when dust is measured as A_V and 0.7 dex for A_{1500} . The latter value agrees with the difference in cosmic abundances of carbon between the SMC and MW, lending support to the idea that $N(C)$ is the more fundamental measure for the gas-to-dust ratio than $N(H)$.

Our study provides a new perspective regarding the physical underpinnings of the measurements of dust in

our galaxy and beyond, and can be used to inform efforts to model extinction curves, grain size evolution, and attenuation in galaxies.

ACKNOWLEDGMENTS

The authors would like to acknowledge the usefulness of the SciPy (Virtanen et al. 2020) and `extinction` (Barbary 2016) packages in Python.

REFERENCES

- Anders, E., & Grevesse, N. 1989, *GeoCoA*, 53, 197, doi: [10.1016/0016-7037\(89\)90286-X](https://doi.org/10.1016/0016-7037(89)90286-X)
- Barbaro, G., Geminale, A., Mazzei, P., & Congiu, E. 2004, *MNRAS*, 353, 760, doi: [10.1111/j.1365-2966.2004.08107.x](https://doi.org/10.1111/j.1365-2966.2004.08107.x)
- Barbary, K. 2016, `extinction` v0.3.0
- Bohlin, R. C., Savage, B. D., & Drake, J. F. 1978, *ApJ*, 224, 132, doi: [10.1086/156357](https://doi.org/10.1086/156357)
- Bohren, C. F., & Huffman, D. R. 1983, *Absorption and scattering of light by small particles*
- Cardelli, J. A., Clayton, G. C., & Mathis, J. S. 1989, *ApJ*, 345, 245, doi: [10.1086/167900](https://doi.org/10.1086/167900)
- Clayton, G. C., & Martin, P. G. 1985, *ApJ*, 288, 558, doi: [10.1086/162821](https://doi.org/10.1086/162821)
- Clayton, G. C., Wolff, M. J., Gordon, K. D., & Misselt, K. A. 2000, in *Astronomical Society of the Pacific Conference Series*, Vol. 196, *Thermal Emission Spectroscopy and Analysis of Dust, Disks, and Regoliths*, ed. M. L. Sitko, A. L. Sprague, & D. K. Lynch, 41–49
- Draine, B. T. 2003, *ARA&A*, 41, 241, doi: [10.1146/annurev.astro.41.011802.094840](https://doi.org/10.1146/annurev.astro.41.011802.094840)
- Fitzpatrick, E. L. 1999, *PASP*, 111, 63, doi: [10.1086/316293](https://doi.org/10.1086/316293)
- Fitzpatrick, E. L., & Massa, D. 1990, *ApJS*, 72, 163, doi: [10.1086/191413](https://doi.org/10.1086/191413)
- . 2007, *ApJ*, 663, 320, doi: [10.1086/518158](https://doi.org/10.1086/518158)
- . 2009, *ApJ*, 699, 1209, doi: [10.1088/0004-637X/699/2/1209](https://doi.org/10.1088/0004-637X/699/2/1209)
- Galliano, F., Galametz, M., & Jones, A. P. 2018, *ARA&A*, 56, 673, doi: [10.1146/annurev-astro-081817-051900](https://doi.org/10.1146/annurev-astro-081817-051900)
- Gordon, K. D., & Clayton, G. C. 1998, *ApJ*, 500, 816, doi: [10.1086/305774](https://doi.org/10.1086/305774)
- Gordon, K. D., Clayton, G. C., Misselt, K. A., Landolt, A. U., & Wolff, M. J. 2003, *ApJ*, 594, 279, doi: [10.1086/376774](https://doi.org/10.1086/376774)
- Gudennavar, S. B., Bubbly, S. G., Preethi, K., & Murthy, J. 2012, *ApJS*, 199, 8, doi: [10.1088/0067-0049/199/1/8](https://doi.org/10.1088/0067-0049/199/1/8)
- Hollenbach, D., & Salpeter, E. E. 1971, *ApJ*, 163, 155, doi: [10.1086/150754](https://doi.org/10.1086/150754)
- Jones, T. J., & Hyland, A. R. 1980, *MNRAS*, 192, 359, doi: [10.1093/mnras/192.3.359](https://doi.org/10.1093/mnras/192.3.359)
- Jura, M. 1980, *ApJ*, 235, 63, doi: [10.1086/157610](https://doi.org/10.1086/157610)
- Kahre, L., Walterbos, R. A., Kim, H., et al. 2018, *ApJ*, 855, 133, doi: [10.3847/1538-4357/aab101](https://doi.org/10.3847/1538-4357/aab101)
- Kim, S.-H., & Martin, P. G. 1996, *ApJ*, 462, 296, doi: [10.1086/177151](https://doi.org/10.1086/177151)
- Koornneef, J. 1983, *A&A*, 500, 247
- Liszt, H. 2014, *ApJ*, 783, 17, doi: [10.1088/0004-637X/783/1/17](https://doi.org/10.1088/0004-637X/783/1/17)
- Martin, P. G. 1978, *Cosmic dust. Its impact on astronomy*
- Martin, P. G., & Whittet, D. C. B. 1990, *ApJ*, 357, 113, doi: [10.1086/168896](https://doi.org/10.1086/168896)
- Mathis, J. S. 1990, *ARA&A*, 28, 37, doi: [10.1146/annurev.aa.28.090190.000345](https://doi.org/10.1146/annurev.aa.28.090190.000345)
- Naoi, T., Tamura, M., Nagata, T., et al. 2007, *ApJ*, 658, 1114, doi: [10.1086/512030](https://doi.org/10.1086/512030)
- Nogueras-Lara, F., Gallego-Calvente, A. T., Dong, H., et al. 2018, *A&A*, 610, A83, doi: [10.1051/0004-6361/201732002](https://doi.org/10.1051/0004-6361/201732002)
- Purcell, E. M. 1969, *ApJ*, 158, 433, doi: [10.1086/150207](https://doi.org/10.1086/150207)
- Rachford, B. L., Snow, T. P., Tumlinson, J., et al. 2002, *ApJ*, 577, 221, doi: [10.1086/342146](https://doi.org/10.1086/342146)
- Rachford, B. L., Snow, T. P., Destree, J. D., et al. 2009, *ApJS*, 180, 125, doi: [10.1088/0067-0049/180/1/125](https://doi.org/10.1088/0067-0049/180/1/125)
- Rémy-Ruyer, A., Madden, S. C., Galliano, F., et al. 2014, *A&A*, 563, A31, doi: [10.1051/0004-6361/201322803](https://doi.org/10.1051/0004-6361/201322803)
- Rieke, G. H., & Lebofsky, M. J. 1985, *ApJ*, 288, 618, doi: [10.1086/162827](https://doi.org/10.1086/162827)
- Roman-Duval, J., Jenkins, E. B., Williams, B., et al. 2019, *ApJ*, 871, 151, doi: [10.3847/1538-4357/aaf8bb](https://doi.org/10.3847/1538-4357/aaf8bb)
- Russell, S. C., & Dopita, M. A. 1992, *ApJ*, 384, 508, doi: [10.1086/170893](https://doi.org/10.1086/170893)
- Salim, S., & Narayanan, D. 2020, *ARA&A*, 58, 529, doi: [10.1146/annurev-astro-032620-021933](https://doi.org/10.1146/annurev-astro-032620-021933)
- Savage, B. D., Bohlin, R. C., Drake, J. F., & Budich, W. 1977, *ApJ*, 216, 291, doi: [10.1086/155471](https://doi.org/10.1086/155471)
- Schlafly, E. F., Meisner, A. M., Stutz, A. M., et al. 2016, *ApJ*, 821, 78, doi: [10.3847/0004-637X/821/2/78](https://doi.org/10.3847/0004-637X/821/2/78)

- Schlegel, D. J., Finkbeiner, D. P., & Davis, M. 1998, *ApJ*, 500, 525, doi: [10.1086/305772](https://doi.org/10.1086/305772)
- Smith, R. G. 1987, *MNRAS*, 227, 943, doi: [10.1093/mnras/227.4.943](https://doi.org/10.1093/mnras/227.4.943)
- Toribio San Cipriano, L., Domínguez-Guzmán, G., Esteban, C., et al. 2017, *MNRAS*, 467, 3759, doi: [10.1093/mnras/stx328](https://doi.org/10.1093/mnras/stx328)
- Valencic, L. A., Clayton, G. C., & Gordon, K. D. 2004, *ApJ*, 616, 912, doi: [10.1086/424922](https://doi.org/10.1086/424922)
- Virtanen, P., Gommers, R., Oliphant, T. E., et al. 2020, *Nature Methods*, 17, 261
- Vuong, M. H., Montmerle, T., Grosso, N., et al. 2003, *A&A*, 408, 581, doi: [10.1051/0004-6361:20030942](https://doi.org/10.1051/0004-6361:20030942)
- Wang, S., & Chen, X. 2019, *ApJ*, 877, 116, doi: [10.3847/1538-4357/ab1c61](https://doi.org/10.3847/1538-4357/ab1c61)
- Wang, S., & Jiang, B. W. 2014, arXiv e-prints, arXiv:1405.1171. <https://arxiv.org/abs/1405.1171>
- Welty, D. E., Xue, R., & Wong, T. 2012, *ApJ*, 745, 173, doi: [10.1088/0004-637X/745/2/173](https://doi.org/10.1088/0004-637X/745/2/173)
- Whittet, D. C. B. 1992, *Dust in the galactic environment*
- Zasowski, G., Majewski, S. R., Indebetouw, R., et al. 2009, *ApJ*, 707, 510, doi: [10.1088/0004-637X/707/1/510](https://doi.org/10.1088/0004-637X/707/1/510)
- Zhu, H., Tian, W., Li, A., & Zhang, M. 2017, *MNRAS*, 471, 3494, doi: [10.1093/mnras/stx1580](https://doi.org/10.1093/mnras/stx1580)